EE-2

Millimeter Wave Heterojunction MITATT Diodes *

N.S. Dogan†, J.R. East‡, M.E. Elta‡, and G.I. Haddad‡

ABSTRACT

This paper presents a design theory, fabrication procedure and experimental results for heterojunction millimeter wave transit time devices operating in the IMPATT, MITATT or TUNNETT mode. The results show that significant improvements in the efficiency can be achieved by heterojunction structures. The diodes were operated as oscillators between 65 and 93 GHz. A pulsed power output of 50mw and RF conversion efficiency of 2.4 percent was achieved at 72 GHz.

I. INTRODUCTION

There has been rapid progress in the two terminal transit time device field since negative resistance structures were first proposed. The progress achieved to date is due to improvements in material preparation such as molecular beam epitaxy, circuit design, improved packaging and heat sink technology, and the development of excellent theoretical models. However, the high frequency performance of GaAs IMPATT mode devices is limited. Several reasons have been given for these high frequency limitations. Skin effect loss, series resistance, package effects, circuit matching problems, injected pulse spreading and the saturation of the ionization rates at high electric fields are all important. GaAs IMPATT mode devices have been built at 60 GHz with good efficiencies [1]. Above 60 GHz, the performance of GaAs IMPATT diodes deteriorates rapidly.

Two potential improvements are tunneling injection and velocity modulation. Tunneling current can be incorporated into the avalanche breakdown to reduce the inherently high noise level and to improve the high-frequency performance of GaAs diodes. Nishizawa et al [2], obtained oscillations in the 100 to 248 GHz frequency range from $p^+n^+nn^+$ GaAs diodes with strong tunneling reverse-bias characteristics. Elta et al. [3] reported oscillations from MITATT GaAs diodes at 150 GHz with 3 mw output power. Velocity modulation can be used to modify the induced current in transit-time devices. Adlerstein et al [4] proposed the DOVETT (double- velocity transit-time structure. The DOVETT has two materials with different saturation velocities in the device drift region. The performance of MITATT and TUNNETT diodes can be improved significantly by using double-velocity characteristics.

The remaining sections of this paper will describe the analysis, fabrication and experimental evaluation of homojunction and heterojunction transit time devices. An approximate large-signal analysis of the structures is given in section II. A device fabrication sequence is described in section III. The characteristics of the devices and their RF results are presented in section IV. The overall results are summarized in section V.

II. Approximate Large-Signal Analysis

An approximate large-signal analysis for heterostructure transit-time devices will be presented in this section. The voltage and current waveforms are idealized by assuming saturated velocities and neglect-

*This work was supported by the Naval Research Laboratory.
†Department of Electrical Engineering Washington State University
‡Center for High-Frequency Microelectronics, Department of Electrical Engineering and Computer Science, The University of Michigan

0149-645X/87/0000-0973$01.00 © 1987 IEEE

ing diffusion to obtain analytic expressions for the power and efficiency. The model can be used to optimize the dimensions and material parameters for a variety of homojunction, single heterojunction(GaAlAs-GaAs) and double heterojunction (GaAlAs-GaAs-GaAlAs) structures. The results of the power and efficiency analysis are presented for single and double heterojunction structures.

Figures 1 and 2 show the structure, terminal voltage, injected current and induced current waveforms for double and single heterojunction transit time diodes. The angles θ_m and θ_w depend on the injection mechanism. θ_m is approximately 90 degrees for a tunnel injection process and approximately 180 degrees for an avalanche process. The injection process in turn depends on the properties of the generation region and on the operating conditions. θ_d is the total drift transit angle. Since the induced current is directly proportional to the saturated velocities of the carriers in the drift regions. the current ratio in two different regions can be expressed as

$$\frac{I_2}{I_1} = \frac{\vartheta_{2sat}}{\vartheta_{1sat}} \tag{1}$$

where I_2 and ϑ_{2sat} are the current and saturated velocity of carriers in Region 2 (GaAs) and I_1, and ϑ_{1sat} are the current and saturated velocity of carriers in Region 1 (GaAlAs). The RF power is

$$I_{dc} = \int_o^{2\pi} I_{ind}(\omega t) d(\omega t) \quad . \tag{2}$$

The device efficiency is the ratio of the RF and the DC power. It depends on the RF voltage, and DC voltage and the shape of the induced current waveform.

A computer program to calculate the optimum angles and the corresponding maximum efficiency was written. Since the injection angle θ_m and pulse width θ_w are constant for a given device and operating condition, the device structure variables θ_{h1}, θ_{h2} and θ_d can be chose to maximize the efficiency. Table 1 gives the numerical results for TUNNETT, MITATT and IMPATT heterojunction diodes. The results show that the efficiency for MITATT and TUNNETT diodes can be improved significantly if heterojunction diodes are used. The first set of data in Table 1 is for the idealized case where θ_w is zero. In the second set of date, the injection angles and pulse widths are taken from Elta et al [5]. The numerical results presented in Table 1 can be used as a guideline for the design of heterojunction devices.

III. DEVICE FABRICATION

A wafer thinning and fabrication process for small GaAs structures is shown in figure 3. The MBE grown wafers are first lapped and polished to remove indium from the back side. Most of the remaining GaAs is then removed by chemical bubble etching. The apparatus used for the bubble etching of GaAs is shown in Fig. 4. A series of etching and metallization steps are then used to define the final diode structure. The fabrication sequence is: (a) mesa etching, (2) rim etching, (c) ohmic or Schottky contact metallization, (d) heat sink plating, (e) back side etching, (f) ohmic contact metallization and (g) final mesa etching. The final active device contact will be on the top side of the wafer as shown in figure 3. Steps a and b form depth stops on the epitaxial side of the semiconductor wafer which are used in step e as a thickness gauge. Figure 5 shows a scanning electron microscope photograph of a fabricated GaAs diode

IV. DEVICE CHARACTERIZATION AND RF RESULTS

A range of device operation from avalanche to tunnel injection is possible in transit time devices. A series of measurements was made on an MBE grown test wafer. The injection region of the diode was etched to different thicknesses. Diodes from these different regions were probed and electrical characteristics from near avalanche to tunneling were obtained. Using the information obtained from the test sample, diodes were fabricated from a $p^+ - n^+$ wafer the doping profile shown in Fig. 6. These diodes had a typical operating voltage of 13 volts at 200 mA bias current. The diodes were bonded with quartz standoffs. Fig. 7 shows a scanning electron microscope photograph of the double-quartz-standoff package. The V-band oscillator circuit in unassembled form is shown in figure 8. The RF performance is shown in figure 9.

VII. CONCLUSIONS

This paper describes an approximate large-signal design theory, fabrication techniques and experimental results for millimeter wave transit time devices. The approximate large-signal analysis was used to investigate the power and efficiency of heterojunction transit-time devices. The analysis results show that significant improvement can be achieved for MITATT and TUNNETT devices by using heterostructures for velocity modulation. A device fabrication process which employs a novel wafer thinning technique was presented in detail. This technique allowed the fabrication of millimeter-wave diodes with GaAs thickness of 1.5 microns with excellent yield. The resulting devices produced approximately 50 mw and operated between 60 and 90 GHz. The results presented here are preliminary. With better circuit design and doping profile optimization much better RF performance is expected.

ACKNOWLEDGEMENT

The authors would like to thank Dr. Hadis Morkoc for supplying the MBE wafers used in this work.

References

[1] M. G. Adlerstein and S. L. G. Chu. "GaAs IMPATT diodes for 60 GHz," *IEEE Electron Device Letters,* Vol. EDL-5, No. 3, pp. 97-98, March 1984.

[2] J. Nishizawa, K. Motoya and Y. Okuno. "GaAs TUNNETT Diodes," *IEEE Trans. on Microwave Theory and Techniques,* Vol. MTT-20, No. 12, pp. 1029- 1035, December 1978.

[3] M. E. Elta, H. R. Fetterman, W. V. Macropoulos and J. .J. Lambert. "150 GHz GaAs MITATT Source," *IEEE Electron Device Letters,* Vol. EDL-1, No. 6, pp. 115-116, June 1980.

[4] M. G. Adlerstein and H. Statz. "Double-velocity IMPATT Diodes," *IEEE Trans. on Electronic Devices,* Vol. ED-26, No. 5, pp. 43-45, May 1979.

[5] M. E. Elta and G. I. Haddad. "High- Frequency Limitations of IMPATT, MITATT, and TUNNETT Mode Devices," *IEEE Trans. on Microwave Theory and Techniques,* Vol. MTT-27, No. 5, pp. 442-449, May 1979.

Numerical Results for TUNNETT, MITATT and IMPATT Heterojunction Diodes

	Frequency (GHz)	Diode Mode	Injection Angle θ_m (Degrees)	Pulse Width θ_w (Degrees)	Drift Angle θ_D (Degrees)	Junction Angle θ_h (Degrees)	Normalized Efficiency $\alpha = 3$ (Heterojunction)	Normalized Efficiency $\alpha = 1$ (Homojunction)	Relative Efficiency Improvement Over Homojunction (Percent)
a=1	Ideal	IMPATT	180.00	0	133.5626	--	--	- 0.7246	15
a=3	Ideal	IMPATT	180.00	0	123.2198	236.7503	- 0.8366	--	
a=1	Ideal	TUNNETT	90.00	0	257.4526	--	--	- 0.2172	138
a=3	Ideal	TUNNETT	90.00	0	238.8700	211.1002	- 0.5170	--	
a=1	Ideal	MITATT	135.00	0	197.4531	--	--	- 0.4625	46
a=3	Ideal	MITATT	135.00	0	182.4843	222.4858	- 0.6758	--	
a=1	10	IMPATT*	180.00	75.0	133.5626	--	--	- 0.6740	15
a=3	10	IMPATT*	180.00	75.0	123.2198	199.2790	- 0.7781	--	
a=1	100	TUNNETT*	110.1509	75.0	211.1745	--	--	- 0.2978	83
a=3	100	TUNNETT*	110.1509	75.0	214.0361	178.3098	- 0.5442	--	
a=1	100	MITATT*	164.8453	93.0023	155.4120	--	--	- 0.5714	85
a=3	100	MITATT*	164.8453	93.0023	143.4385	185.2138	- 0.7016	--	
a=1	100	IMPATT*	180.00		134.0114	--	--	- 0.4982	35
a=3	100	IMPATT*	180.00		103.2965	222.1783	- 0.6714	--	

*Data taken from Elta.[11]

Table 1. Numerical Results

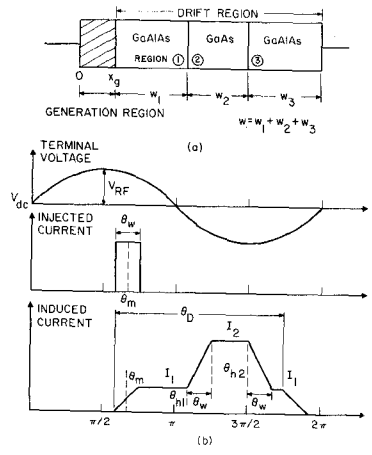

Figure 1. Double Heterojunction Diode Structure and Waveforms

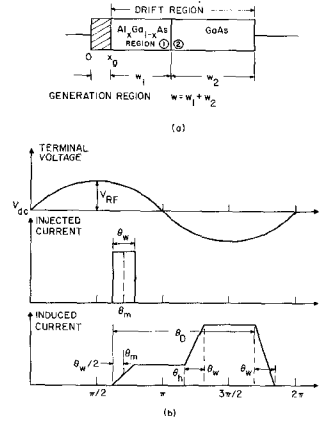

Figure 2. Single Heterojunction Diode Structure and Waveforms

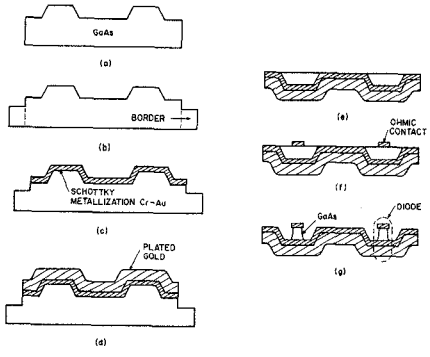

Figure 3. Diode Fabrication Sequence

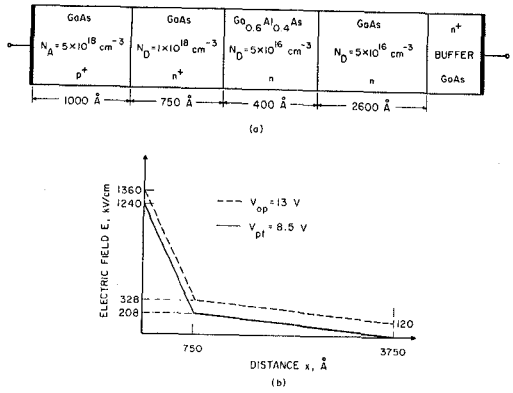

Figure 6. Diode Structure

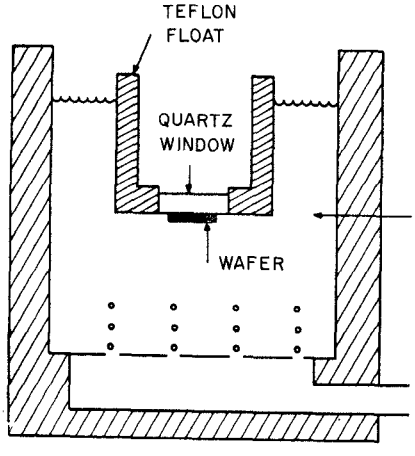

Figure 4. GaAs Etcher

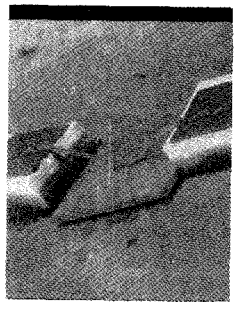

Figure 7. SEM Photograph of Fabricated Diode

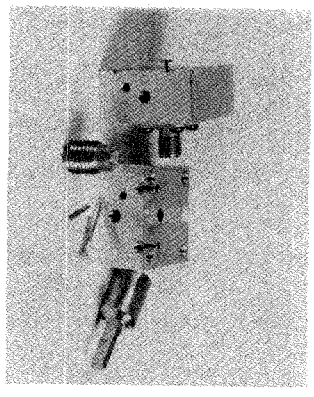

Figure 8. Oscillator Circuit

Figure 5. SEM Photograph of Fabricated Diode

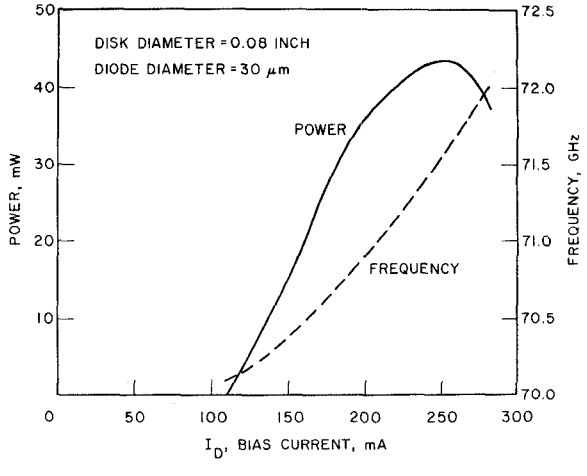

Figure 9. RF Performance